



The Effect of Ambient Pressure and Gas–Liquid Ratio on the Spray Characteristics of an Effervescent Atomizer

Chen Chen¹ · Xiaofan Gong¹ · Yunfei Wang¹ · Xiujie He²

Received: 19 March 2023 / Revised: 6 June 2023 / Accepted: 10 June 2023 / Published online: 19 July 2023
© The Author(s), under exclusive licence to The Korean Society for Aeronautical & Space Sciences 2023

Abstract

To study spray characteristics of an effervescent atomizer, phase Doppler image (PDI) was used to measure diameter distribution, axial velocity distribution and diameter-velocity correlation. The effects of gas–liquid ratio by mass (GLR) and ambient pressure on atomization characteristics were studied experimentally. By increasing the GLR, not only does the mode of droplet diameter decrease, but also the proportion of these droplets in the total droplets increases. Accordingly, the proportion of droplets with a diameter of 59 μm reaches 5.6% at $\text{GLR} = 6\%$. Meanwhile, the upward trend of the cumulative probability curve of droplet size decreases with an increase of GLR. In addition, as the GLR increases, the droplet velocity increases significantly. Moreover, smaller droplets have broader velocity distributions. Similarly, the lower the ambient pressure, the higher the proportion of small droplets. Additionally, the droplet size distribution is highly uneven. Furthermore, the SMD and axial velocity decreases rapidly with increasing radial distance for the same ambient pressure.

Keywords Effervescent atomizer · Spray characteristics · Probability density of droplet size

1 Introduction

The effervescent atomizer has many advantages, such as low operating pressure, simple structure, less gas consumption, and low cost [1–4]. The effervescent atomization technology has been widely studied and applied in various fields such as liquid fuel combustion [5], spray drying [6], medical treatment [7], fire extinguishing [8], and surface spraying [9]. Effervescent atomization is an efficient and cost-effective technology derived from traditional atomization. It involves injecting gas and liquid into a mixing chamber to create a gas–liquid two-phase flow. The droplet formation in effervescent atomization is caused by gas expansion at the exit orifice [10]. When the pressure inside the atomizer is greater than the ambient pressure, the bubble rapidly expands and bursts due to the sudden pressure drop within a very short

period of time after it exits the atomizer. Thus, the liquid film breaks into liquid filaments or smaller liquid drops.

In studying the atomization process of an effervescent atomizer, researchers have focused mainly on the internal flow and the spray characteristics beyond the exit. Avulapati et al. [11] observed that the spray was more unstable at low gas liquid ratio (GLR) of 1.7%. It tended to be stable at high GLR of 10%, where annular flow was observed. Kourmatzis et al. [12, 13] used a high-speed camera to record the near-field atomization. When the GLR reached 0.4%, the internal flow pattern changed from bubble to slug flow. At this point, the liquid column at the exit started to break apart due to the expansion of bubbles. Li et al. [14] found that the flow pattern transition in the mixing chamber was closely related to the droplet distribution through experiments. The annular flow produced a thinner liquid film and finer droplets. Konstantinov et al. [15] analyzed different atomization methods. Compared to other traditional atomization methods, smaller droplets are observed in effervescent atomization. The external field achieves the best atomization performance with bubbly flow in an orifice. Ochowiak et al. [16] proposed that the discharge coefficient (the ratio of the actual mass flow rate of the fluid to the theoretical mass flow rate of the fluid) of an effervescent atomizer decreased with an increase of liquid viscosity. At the same time, the lower the GLR, the greater

✉ Xiujie He
hxj_83@163.com

¹ School of Automotive and Traffic Engineering, Jiangsu University, No. 301, Xuefu Road, Zhenjiang City, Jiangsu Province, People's Republic of China

² School of Power and Energy, Northwestern Polytechnical University, No. 1, Dongxiang Road, Xian City, Shanxi Province, People's Republic of China

the effect of viscosity. Hammad et al. [17] designed a variety of effervescent atomizers with distinct structures. It was observed that the discharge coefficient was not affected by the internal flow pattern. Moreover, the discharge coefficient was more sensitive to viscosity at low GLR.

In judging the effectiveness of atomization, many factors need to be taken into account. The experimental results of Sun et al. [18, 19] revealed that the design of the effervescent atomizer has an impact on the instability of the spray. The spray was more consistent when the air inlet was distant from the orifice. Additionally, a narrow orifice could generate a more consistent atomization cone angle. Huang et al. [20] measured the droplet size and velocity with the aid of an LDV/PDA (laser doppler velocimetry/ phase doppler anemometry) system. The droplets were minute and the axial velocity was high under high operating pressure. Zaremba et al. [21] summarized the mechanism of droplet breaking. As the gas flow increased, the frequency of bubble breakup was higher, resulting in a more uniform spray. At the same time, the droplet size along the central axis of the spray was relatively small. Ramamurthi et al. [22] observed that in slug flow the atomization effect was poor due to the intermittent flow of large bubbles. The annular flow gradually stabilized the atomization cone angle, which caused the Sauter mean diameter (SMD) to gradually decrease. Mohammadi et al. [23] conducted experimental and numerical studies on the spray characteristics and droplet distribution. Both the GLR and the inlet pressure had a significant influence on the droplet diameter. Additionally, an increase of liquid flow rate caused the density of the larger droplet size to increase rapidly.

A large amount of experiments and numerical simulations have been conducted on effervescent atomizers. However, there are only a few reports on the influence of ambient pressure on the distribution characteristics of external flow field. In the constant volume bomb experiment of internal combustion engine, it usually presents as pressure atomization without air injection, with a high ambient pressure but only for microsecond-level experiments for spray evolution or spray pattern [24–26]. For the effervescent atomizer, the addition of gas assistance causes the ambient pressure to fluctuate. PDA has a great advantage for high measurement accuracy. However, the single point measurement of phase Doppler image (PDI) or PDA requires a considerable amount of time to complete the target measurement points. When the nozzle flow rate reaches tens or even hundreds of grams per second, it is considered a very large flow rate for the effervescent atomizer in the experiment. The spread of the droplets is so intense that it covers the surface of the optical window with droplets, making it difficult to carry out routine measurements. It brings great challenges for the design of constant volume bomb and ambient pressure adjustment.

Furthermore, the correlation between diameter and velocity is of great importance for the analysis of the atomization

process and engineering application. Nevertheless, most of the current data on droplet size only concentrate on SMD [27, 28]. Studies by Frederik et al. [10] and Nielsen et al. [29] showed that the SMD had no direct relation to the mixing chamber structure. But the mixing chamber structure has an effect on the flow pattern and thus influence the droplet diameter. Sovani et al. [30] summarized that the SMD was most significantly influenced by GLR. Cejpek [31] concluded that SMD is also mainly affected by GLR. Meanwhile, the empirical formula of SMD about GLR is obtained. Liu [32] found that the increase of injection pressure and GLR can reduce the SMD in the experiment. Wittner [28] also found that the droplet size decreases with the increase of injection pressure. However, due to the large momentum of liquid–gas interaction, the effect of injection pressure on SMD decreases with the increase of GLR. In fact, the injection pressure will increase with the increase of liquid and gas flow. Furthermore, the change of GLR is also by adjusting the flow of liquid and gas in the experiments. Therefore, GLR can better describe the experimental conditions. In this paper, the effects of GLR and ambient pressure on the diameter distribution, axial velocity distribution and diameter-velocity correlation of an effervescent atomizer are explored experimentally. The time distribution of the droplet size and axial velocity is analyzed. Additionally, the effect of the GLR and ambient pressure on the probability density of the droplet size is systematically examined.

2 Experimental Methods

As illustrated in Fig. 1, the experimental system consists of a gas–liquid supply system, an atomization system, an optical measurement system, and a data acquisition system. The structural parameters and conditioning process of the chamber have been thoroughly discussed in [33, 34]. The experiment was filmed through an observation window of an ambient pressure tank. In analyzing measurements of the PDI system, the orifice exit is taken as the origin. The measuring section is set along the injection direction (z -direction). The sampling interval is chosen according to the spray angle. In the experiment, Artium's PDI-300 MD PDI system is utilized. The droplet size measurement range of the system is 0.5–2000 μm , with an accuracy of 0.5 μm . The velocity measurement range is 0–300 m/s, with a measurement accuracy of 1%. The reasons for selecting this system has been introduced in reference [35]. To guarantee the accuracy of the measurement results, the number of collected droplets at each measured point was more than 5000.

The effervescent atomizer utilized in the experiment is depicted in Fig. 2. The application object of the nozzle in this paper is the torch igniter. The torch igniter requires a stable and uniform spray process. Studies have shown that

Fig. 1 Schematic of the experimental setup

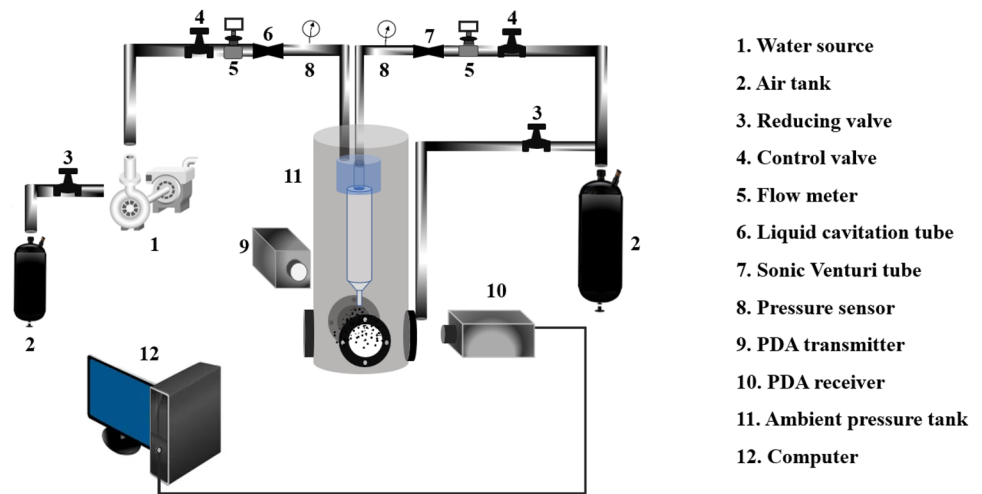
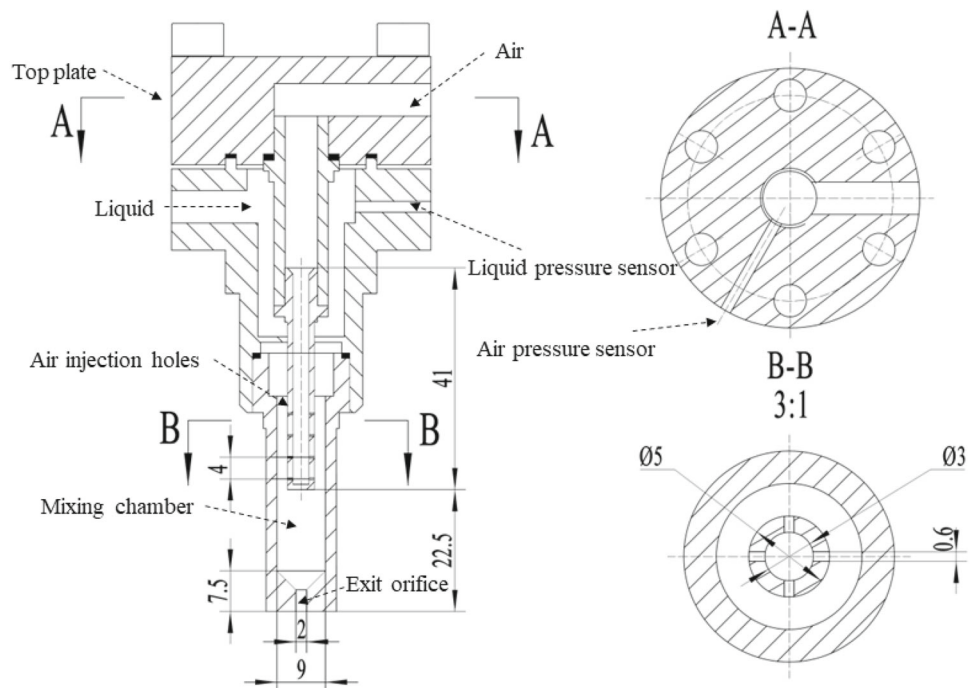


Fig. 2 Internal structure of effervescent atomizer



the flow pattern of outside-in-gas (OIG) atomizer is mostly bubbly flow. An intermittent flow of gas–liquid alternating occurs at the orifice exit, resulting in unstable atomization [5, 6]. The outside-in-liquid (OIL) atomizer is dominated by annular flow pattern, which provides a more stable spray [36]. Therefore, the nozzle used in this experiment is OIL. The center of the liquid chamber is equipped with an air inlet chamber with a diameter of 3 mm. The bottom wall of the inlet chamber has 4 rows of evenly distributed air outlets with diameters of 0.6 mm, amounting to 16 in total. The outlet is connected to the gas–liquid mixing chamber. Pure water and air were employed as experimental working media. In the experiment, the gas enters the inlet chamber from the

top. Simultaneously, pure water enters the gas–liquid mixing chamber from the liquid inlet. Due to the pressure gradient, the gas is forced into the liquid from the outlet to form a two-phase flow. Finally, the gas–liquid two-phase flow is discharged from the orifice with a pressure gradient. The gas duct of the effervescent atomizer is constructed of stainless steel. The gas–liquid mixing chamber is made of stainless steel and transparent acrylic organic glass. The gas mass flow and liquid mass flow is controlled by a venturi tube and liquid cavitation tube during the experiment, respectively. And they are displayed and recorded with a flowmeter, respectively. The liquid flow rate has a constant value of 20 g/s. For axial cross-sectional data measurements, four absolute

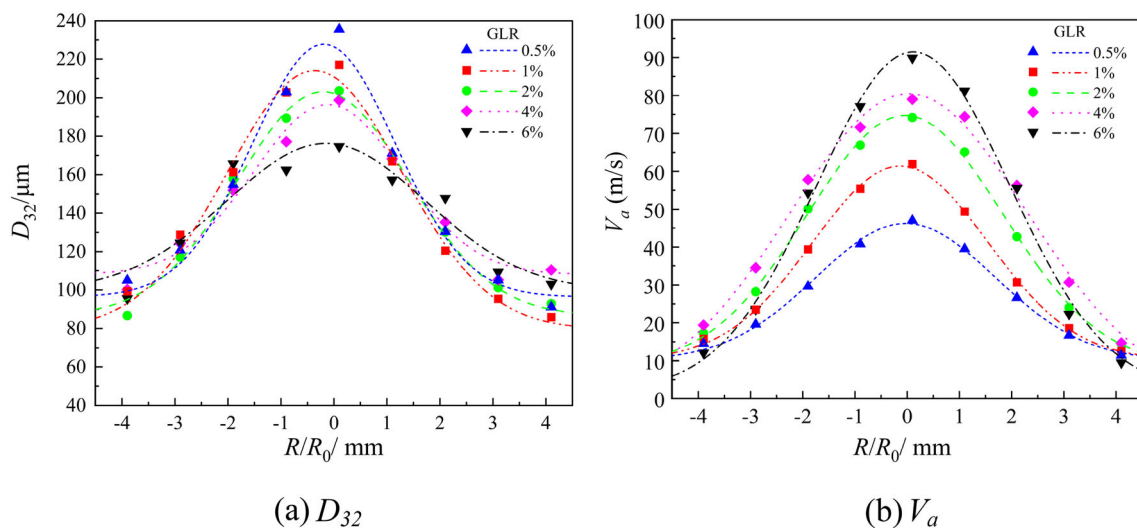


Fig. 3 The distribution of droplet size and axial velocity at axial distance $z = 40$ mm for various values of GLR

ambient pressures (0.1, 0.6, 1.2, and 1.8 MPa) and five different GLRs (0.5%, 1%, 2%, 4%, 6%) were chosen for the experiment.

3 Results and Discussion

3.1 Effect of GLR on Spray Characteristics

Figure 3 show the effect of GLR on the distribution of the droplet size and axial velocity along the radial direction at an axial distance $z = 40$ mm. The change of radial distance is quantitatively represented by the equivalent distance R/R_0 , where, R is the radial distance from the outside of spray to the axis, mm; R_0 is the orifice diameter, mm. Under the same GLR, the maximum droplet diameter is in the center of the spray. The axial velocity distribution shows similar distribution characteristics. In the central region, the breakup of the liquid is mainly dependent on the explosive effect of the bubble and the aerodynamic effect between the droplets and the ambient air. The energy produced by the explosion of the bubbles not only produces droplets of different sizes, but also imparts radial velocity to the droplets [21]. And the axial velocity of the droplets is increased. Smaller droplets are easier to follow the gas to move outward. During the process of outward movement, the droplets are broken again under the action of aerodynamic force. As a result, the droplet diameter gradually shows smaller along the radial direction. Meanwhile, the kinetic energy of droplets decreases for the resistance of air, and the velocity gradually decreases. With the increase of the GLR, the droplet diameter in the central region of the spray decrease. The curve is becoming more gentle in its downward trend.

Figures 4 and 5 show the effect of GLR on the time distribution and probability density of the droplet size at the section at an axial distance $z = 40$ mm. And the droplet size distributions here are number based distributions. The red dotted line represents the value of D_{32} . As can be seen from Fig. 4, most of the droplet sizes for different GLR are in the range 30–100 μm . However, the fraction of droplets within this range is different. The higher the GLR, the larger the fraction of droplets in that size range. As shown in Fig. 5, the diameter of droplets is mainly concentrated around 65 μm , with only 2.2% of the total droplets having this diameter at GLR of 0.5%. However, when the GLR is 6.0%, the droplets with a diameter of 59 μm account for 5.6% of the total. In addition, it can be seen from the Fig. 4 that the D_{32} significantly decreases with the increase of GLR. The number of large droplets significantly decreases with the increase of GLR. And large droplets will increase the value of D_{32} in the calculation formula of D_{32} . As a result, the D_{32} decreases from 236.2 μm under the lowest GLR of 0.5% to 174.6 μm under the highest GLR of 6%. The value of D_{32} has decreased by up to 35.2%.

Figure 6 is a time distribution diagram of the effect of GLR on the axial velocity of droplets at $z = 40$ mm. As can be seen from the figures, the droplet velocity increases significantly as GLR increases. As the gas flow rate increases, the pressure in the mixing chamber increases accordingly, resulting in an increase of the internal–external pressure difference. This, in turn, leads to an increase in the velocity of the outlet and the energy of the bubbles. Consequently, the bubbles have greater bursting energy after ejecting from the orifice, significantly increasing the droplet velocity outside the orifice [37].

Figure 7 illustrates the relationship between droplet velocity and droplet size at $z = 40$ mm for GLR values of 0.5 to

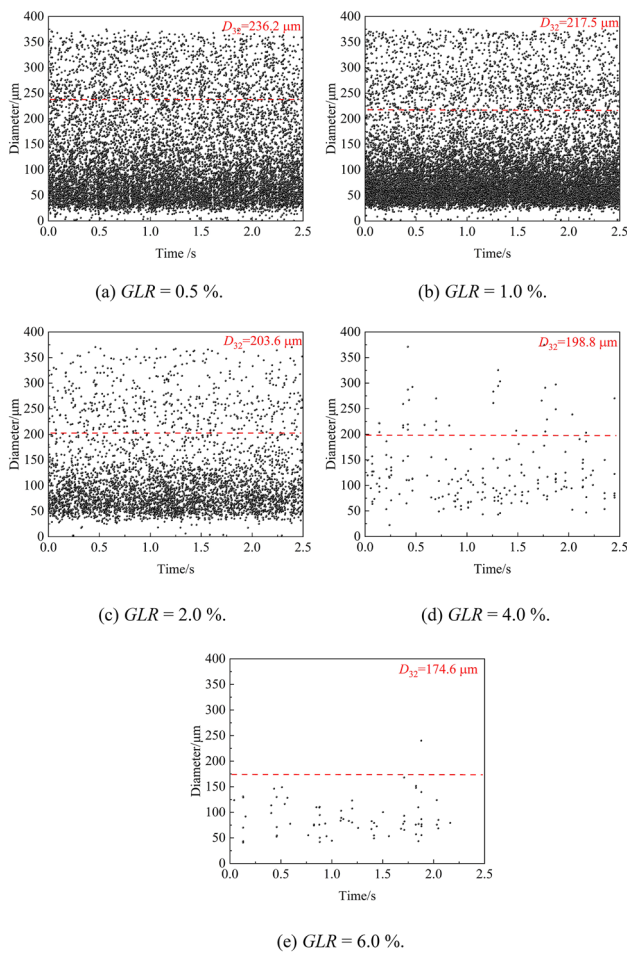


Fig. 4 Time distribution of droplet size at axial distance $z = 40$ mm for various values of GLR ($R/R_0=0$)

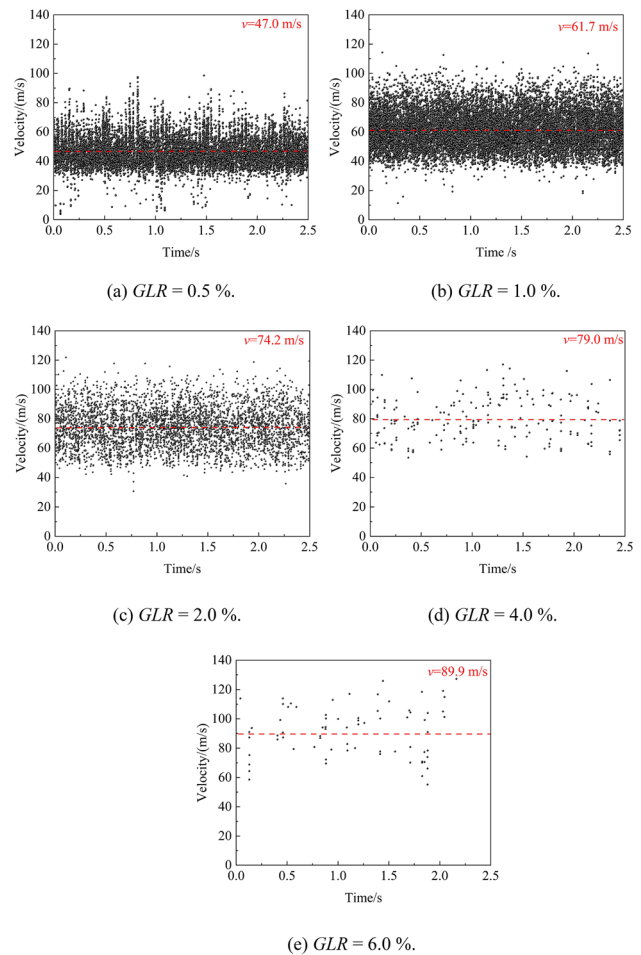


Fig. 6 Time distribution of axial velocity at $z = 40$ mm for various values of GLR ($R/R_0=0$)

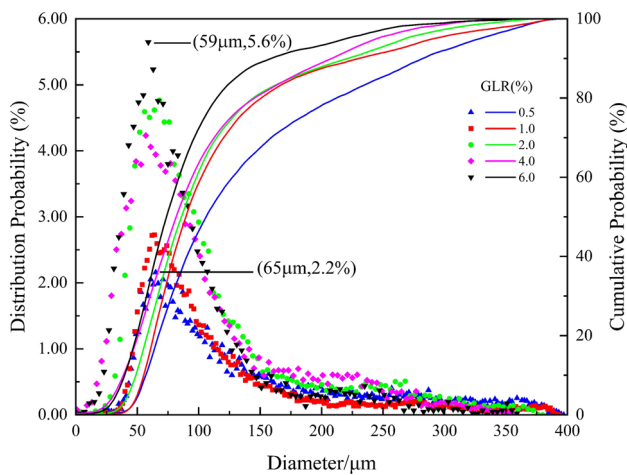


Fig. 5 Probability density of droplet diameter at $z = 40$ mm for various values of GLR ($R/R_0=0$)

6%. The horizontal and vertical red dotted line lines represent the average velocity and D_{32} , respectively. As can be seen from the figure, the smaller the droplet size in the spray

field, the higher the average velocity for all values of GLR. It is noteworthy that this is contrary to the characteristics of droplets in swirl injectors and gas–liquid swirl coaxial injectors. The larger the droplet at the outlet of such an injector, the greater the inertia. Since small droplets have less inertia, their velocity decreases rapidly under the influence of aerodynamic drag. For the effervescent atomizer, by contrast, the fragmentation of the outlet liquid film is mainly achieved by the explosion of bubbles after the bubbles left the orifice [38]. The increase of gas flow represents the increase of inlet velocity. Therefore, the liquid film will have a greater velocity difference with the air after leaving the nozzle exit, resulting in stronger shear force. This causes the liquid film to break into smaller droplets. And the initial velocity is higher. Furthermore, the expansion effect of bubbles will also be more intense for the increase of internal and external pressure difference. Additionally, the inertia of small droplets is smaller than that of large droplets, so the velocity change is more obvious. Therefore, small droplets have very broad velocity distributions.

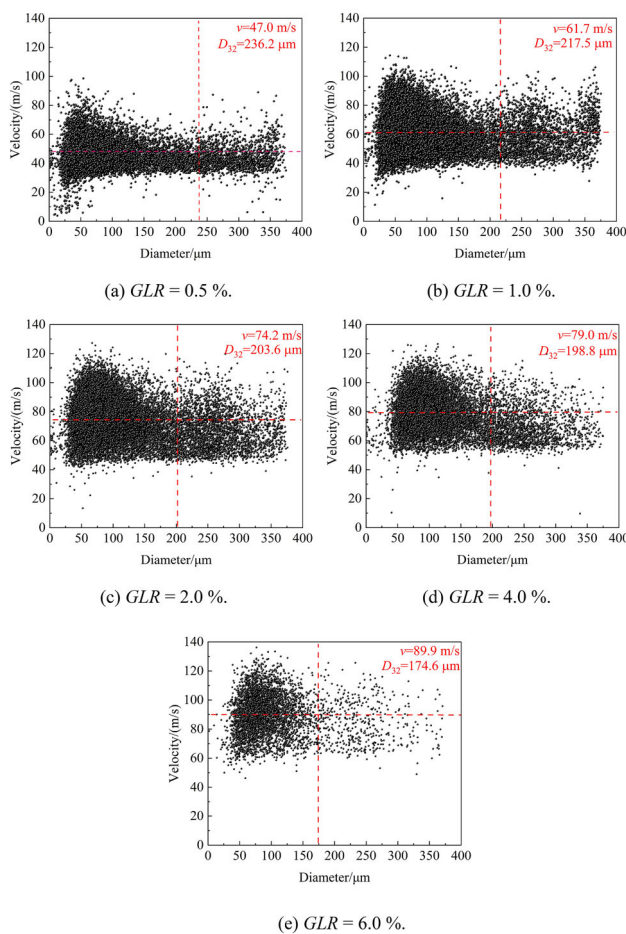


Fig. 7 Relationship of axial velocity and droplet size at $z = 40$ mm for various values of GLR ($R/R_0=0$)

Figure 8 shows the time distribution of droplet size with R/R_0 from axis at $z = 40$ mm and $GLR = 2\%$. As illustrated in this figure, the mode of droplet size increases from 50 μm in Fig. 8a to 65 μm in Fig. 8e along the spray edge to the axial center (The 'mode' here refers to the highest proportion of droplets.). At the same time, the distribution of droplet size is more dispersed, showing an increasing proportion of large droplets. Figure 9 shows the probability density of droplet size at different radial positions at $z = 40$ mm and for $GLR = 2\%$. The maximum probability of droplet size decreases from 10.8% at $R/R_0 = -4$ to 4.9% at $R/R_0 = 0$. It is evident that the upward trend of the cumulative probability distribution curve of droplet size slows down. It results in the SMD gradually increasing in the radial direction, which is in line with the pattern observed in Fig. 3.

Figure 10 shows the time distribution of the axial velocity of droplets on the cross section at $z = 40$ mm and for $GLR = 2\%$. This phenomenon has two primary causes: Firstly, the bubble detonates at the center of the orifice exit, thus providing the droplets at the center with greater explosive energy and higher speed. Secondly, as the droplet diffuses around,

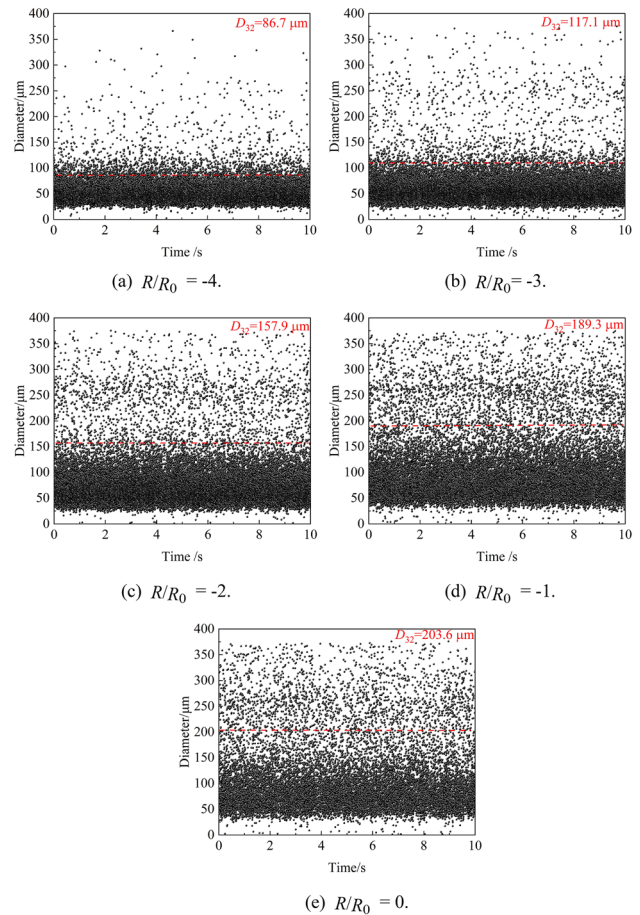


Fig. 8 Time distribution of droplet size on the cross section at $z = 40$ mm ($GLR = 2\%$)

the droplet is impeded by the resistance of the surrounding gas, thus causing its speed to decrease [39, 40]. This behavior can also be found from Fig. 11, which shows the relationship between axial velocity and droplet size. In Fig. 11, the droplet size and velocity at the spray edge are lower than at the axial position.

3.2 Effect of Ambient Pressure on Atomization Characteristics

Four sets of experiments with varying ambient pressure were conducted for a GLR of 4% . Figure 12 displays the temporal distribution of droplet size at $z = 40$ mm. In the experiment, the minimum droplet size and the maximum droplet size were 1 μm and 375 μm, respectively. As shown in Fig. 12, the main distribution range of droplet size is 25 to 370 μm. The lower the ambient pressure, the higher the proportion of small droplets. Furthermore, droplet size distribution is highly irregular. As the ambient pressure increases, the number of droplets of different sizes changes drastically, exhibiting an increasing proportion of large droplets. The

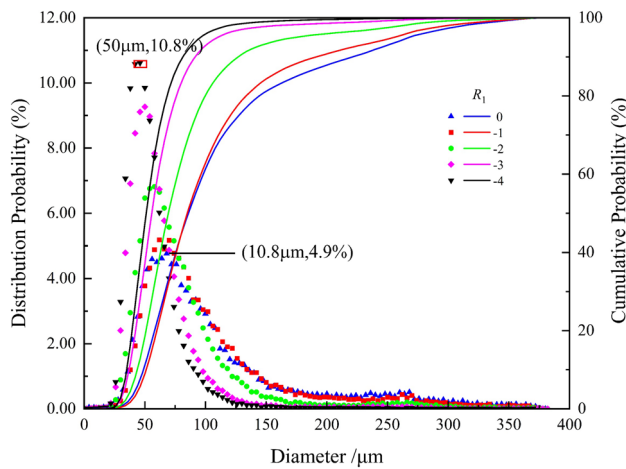


Fig. 9 Probability density of droplet size at $z = 40$ mm (GLR = 2%)

density of the ambient gas increases with the increase of the ambient pressure, resulting in an increase in the resistance of the liquid film. In addition, the pressure difference between the inside and outside of the orifice is smaller, resulting in less energy for bubble expansion and breaking. Therefore, the droplet diameter will be larger under high ambient pressure. This also causes the D_{32} to increase with increasing ambient pressure. It can be seen from the Fig. 12 that D_{32} increased from 198.8 μm at the ambient pressure of 0.1 MPa to 225.7 μm at the ambient pressure of 1.8 MPa.

Under the same conditions, the probability density of droplet size at axial distance $z = 40$ mm from the exit outlet can be seen in Fig. 13. It reveals that droplet size tends to increase with an increase in ambient pressure, thus resulting in fewer droplets of small size. Simultaneously, the slope of the droplet size cumulative probability density curve becomes less steep. Figure 13 summarizes the relationship between droplet distribution and ambient pressure from the data in Fig. 12.

Figure 14 shows the time distribution of axial velocities of droplet size at $z = 40$ mm from the orifice outlet under the same working condition. As can be observed from Fig. 14, the lower the ambient pressure, the broader the range of droplet velocity and the larger the velocity disparities among droplets. Conversely, the higher the ambient pressure, the more concentrated the droplet velocity distribution and the smaller the velocity differences among droplets. Additionally, as the ambient pressure increases, the droplet velocity decreases significantly [41]. When the ambient pressure increases, the air density around the spray increases. Therefore, the aerodynamic drag of the droplet increases, resulting in greater momentum loss. Thus, the axial velocity decreases with the increase of ambient pressure. Due to the increase of ambient pressure, the pressure difference inside and outside the orifice is smaller, resulting in less energy for bubble expansion and breakage. Therefore, the droplet

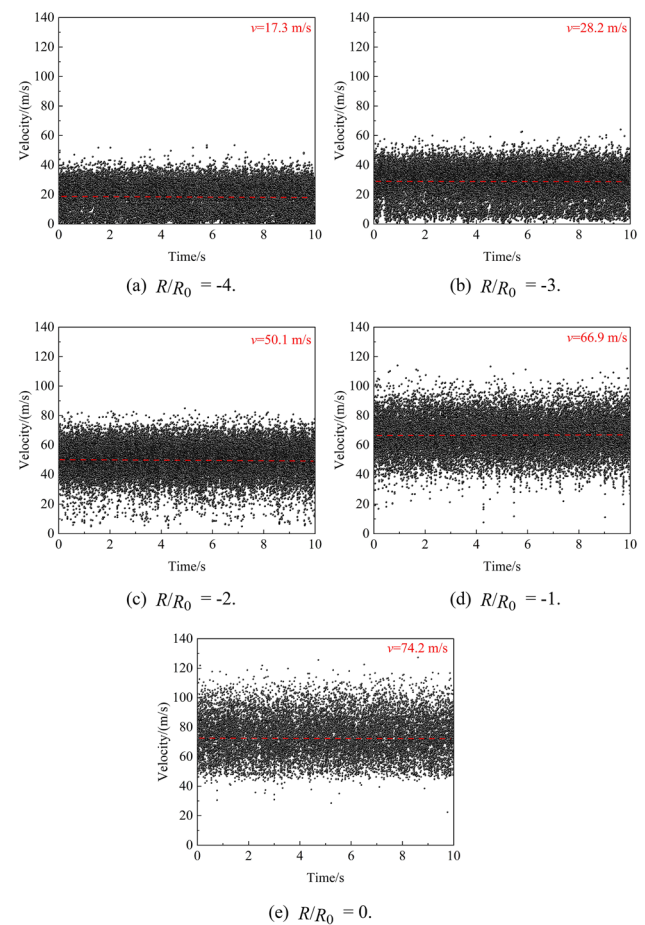


Fig. 10 Time distribution of axial velocity at axial position $z = 40$ mm (GLR = 2%)

diameter will be larger under high ambient pressure. The aerodynamic drag around them is relatively weak for the large inertia of the larger droplets, resulting in a smaller change in velocity. Therefore, the velocity distribution is relatively concentrated. For example, under an ambient pressure of 0.1 MPa, the droplet velocities range from 60 to 120 m/s, with a uniform distribution of droplets of different velocities. However, the velocities for an ambient pressure of 1.8 MPa are significantly lower than for an ambient pressure of 0.1 MPa. And they are concentrated in the 20–40 m/s range.

Figure 15 shows the distribution of droplet size and velocity at $z = 40$ mm for different ambient pressures. As can be seen from Fig. 15, small droplets have a wider velocity distribution than large droplets for different ambient pressures. Taking the ambient pressure of 1.2 MPa as a reference, droplets with a size of 75 μm have velocities in the range of 20–60 m/s, whereas droplets with a size of 300 μm have velocities in the range of 30–60 m/s. Gradually, as the ambient pressure rises, the range of droplet velocities decreases. This is due to the fact that the bubble explosion at the exit

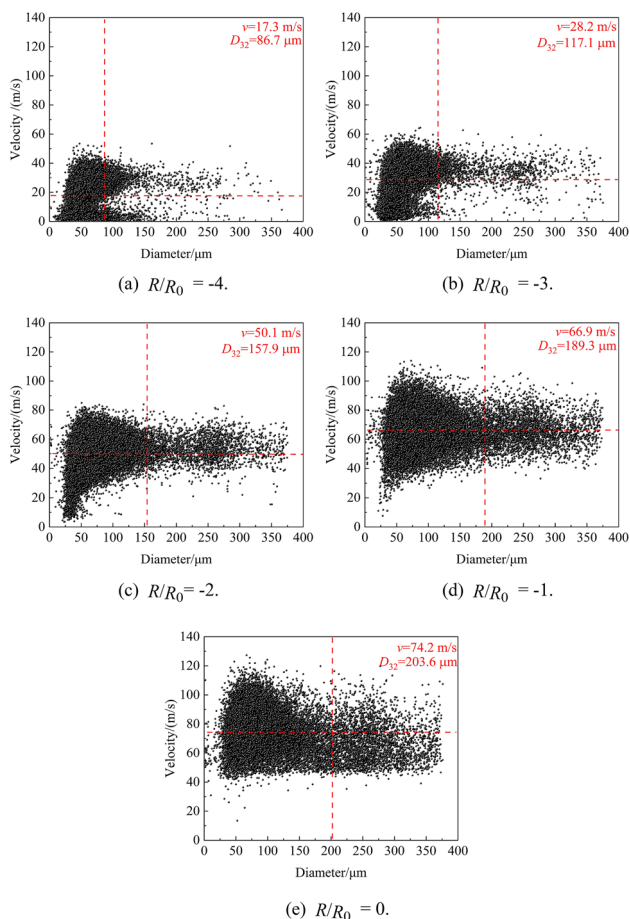


Fig. 11 Relationship between axial velocity and droplet size at axial position $z = 40$ mm (GLR = 2%)

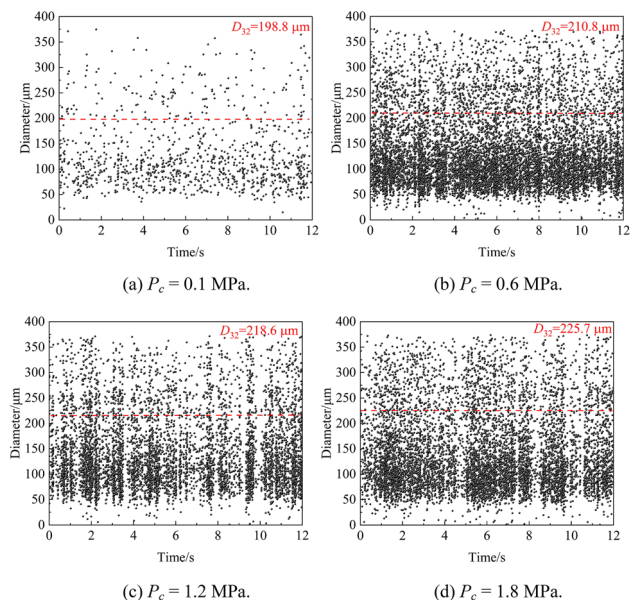


Fig. 12 Time distribution of droplet size at axial distance $z = 40$ mm for various ambient pressures (GLR = 4%, $R/R_0=0$)

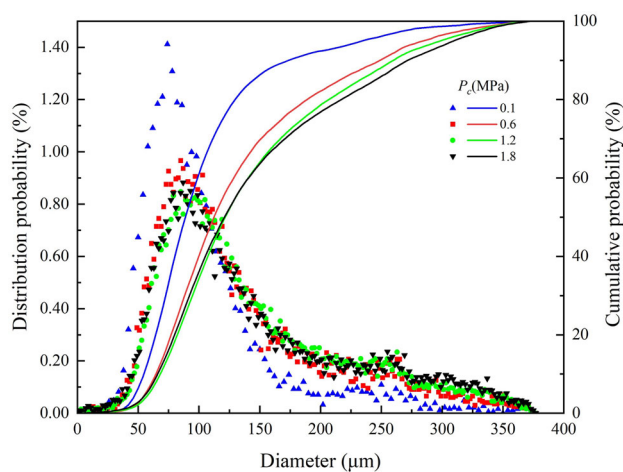


Fig. 13 Probability density of droplet size at an axial distance $z = 40$ mm for various ambient pressures (GLR = 4%, $R/R_0=0$)

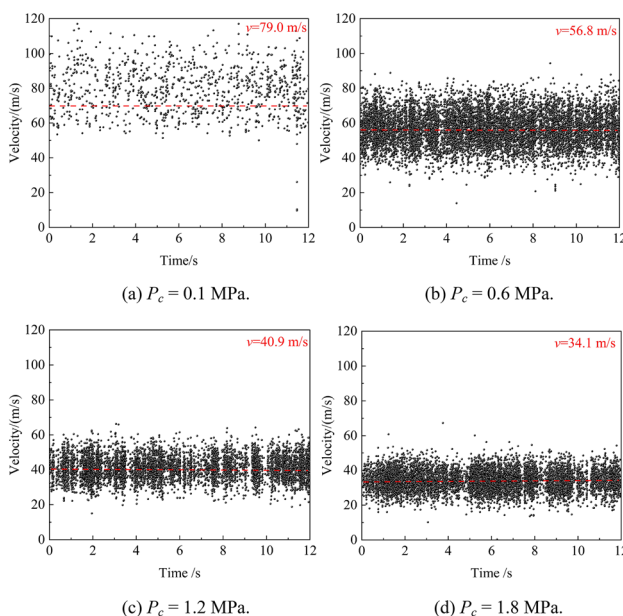


Fig. 14 Time distribution of axial velocities at an axial distance $z = 40$ mm for various ambient pressures (GLR = 4%, $R/R_0=0$)

outlet produces droplets of varying sizes. Smaller droplets, having less inertia, are more susceptible to change in motion. As a result, the velocity distribution of droplets will be wider. On the other hand, larger droplets, with greater inertia, are less affected by aerodynamic drag. Consequently, the speed of large droplets decreases more slowly and their distribution is more concentrated.

From the above analysis, it can be seen that for the same ambient pressure, the SMD and axial velocity decrease rapidly as radial distance increases. Furthermore, the droplet size decreases and the velocity decreases at the edge of the spray. The SMD at the axis increases with an increase

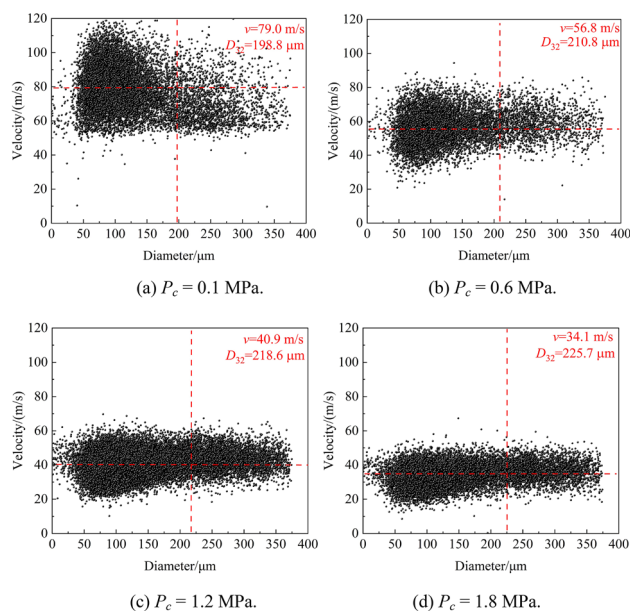


Fig. 15 Relationship between axial velocity and droplet size at an axial distance $z = 40$ mm for various ambient pressures (GLR = 4%, R/R₀=0)

in ambient pressure [42]. By contrast, the axial velocity decreases as ambient pressure increases. Most important, an increase in ambient pressure reduces the axial velocity differences among droplets.

4 Conclusions

This study focused on the effects of GLR and ambient pressure on the atomization characteristics. The droplet size and velocity distributions were measured by PDI system. In contrast to a centrifugal atomizer, the smaller droplets in the spray field of the effervescent atomizer have a higher velocity, and the larger droplets have a lower velocity. The ascending trend of the cumulative probability curve of droplet size decreases with an increase in GLR. The results showed that the SMD increased steadily along the radial direction away from the axis.

It is observed that the velocity distribution of droplets is more concentrated at high ambient pressure. Simultaneously, the velocity difference between droplets becomes smaller. Correspondingly, the slope of the cumulative probability density curve of droplet size decreases with an increase in ambient pressure.

Authors' contributions CC was involved in the methodology, experiments, investigation, writing-original draft, visualization and funding acquisition. XG and YW was involved in the review and editing. XH contributed to the experiments, data curation, writing-original draft, review and editing.

Funding The authors would like to express their sincere thanks for the support from the National Natural Science Foundation of China (No. 12002138), Science and Technology on Scramjet Laboratory Project of China (WDZC614270302207), China Postdoctoral Science Foundation (2022M721377) and Young Elite Scientists Sponsorship Program by Jiangsu Association for Science and Technology (TJ-2022 -057).

Availability of Data and Materials The datasets used or analyzed during the current study are available from the corresponding author on reasonable request.

Declarations

Competing Interests The authors declare that they have no known competing financial interests or personal relationships that could have appeared to influence the work reported in this paper.

Ethical Approval Not applicable.

References

- Jedelsky J, Jicha M, Slama J, Otahal J (2009) Development of an effervescent atomizer for industrial burners. *Energy Fuels* 23(6):6121–6130
- Zhao F, Ren ZB, Xu BB, Zhang HY, Fu C (2019) Brief overview of effervescent atomizer application. *J Phys: Conf Ser* 1300(1):012043
- Sivadas V, Balaji K, Vishwakarma A, Manikandan SR (2020) Experimental characterization of a liquid jet emanating from an effervescent atomizer. *J Fluids Eng* 142(6):064501
- Hammad FA, Sun K, Che Z et al (2021) Internal two-phase flow and spray characteristics of outside-in-liquid twin-fluid atomizers. *Appl Therm Eng* 187:116555
- Gadgil HP, Raghunandan BN (2011) Some features of spray breakup in effervescent atomizers. *Exp Fluids* 50(2):329–338
- Wittner MO, Karbstein HP, Gaukel V (2018) Spray performance and steadiness of an effervescent atomizer and an air-core-liquid-ring atomizer for application in spray drying processes of highly concentrated feeds. *Chem Eng Process Process Intensif* 128:96–102
- Kleinhans A, Georgieva K, Wagner M, Gaukel V, Schuchmann HP (2016) On the characterization of spray unsteadiness and its influence on oil drop breakup during effervescent atomization. *Chem Eng Process Process Intens* 104:212–218
- Huang X, Wang XS, Liao GX (2011) Characterization of an effervescent atomization water mist nozzle and its fire suppression tests. *Proc Combust Inst* 33:2573–2579
- Petersen FJ, Worts O, Schaefer T, Sojka PE (2001) Effervescent atomization of aqueous polymer solutions and dispersions. *Pharm Dev Technol* 6(2):201–210
- Petersen FJ, Worts O, Schaefer T, Sojka PE (2004) Design and atomization properties for an inside-out type effervescent atomizer. *Drug Dev Ind Pharm* 30(3):319–326
- Avulapati MM, Ravikrishna RV (2012) An experimental study on effervescent atomization of bio-oil fuels. *Atomiz Sprays* 22(8):633–685
- Kourmatzis A, Lowe A, Masri AR (2017) Conditioned analysis of effervescent atomization. *J Energy Eng* 143(5):04017019
- Kourmatzis A, Lowe A, Masri AR (2016) Combined effervescent and air-blast atomization of a liquid jet. *Exp Thermal Fluid Sci* 75:66–76

14. Li ZH, Wu YX, Cai CR, Zhang H, Gong YL, Takeno K, Hashiguchi K, Lu JF (2012) Mixing and atomization characteristics in an internal-mixing twin-fluid atomizer. *Fuel* 97:306–314
15. Konstantinov D, Marsh R (2010) Effervescent atomization for industrial energy—technology review. *Atomiz Sprays* 20(6):525–552
16. Ochowiak M (2013) The experimental study on the viscosity effect on the discharge coefficient for effervescent atomizers. *Exp Thermal Fluid Sci* 50:187–192
17. Hammad FA, Sun K, Jedelsky J, Wang TY (2020) The effect of geometrical, operational, mixing methods, and rheological parameters on discharge coefficients of internal mixing twin-fluid atomizers. *Processes* 8(5):563
18. Sun CH, Ning Z, Qiao XQ, Lv M, Zhao J, Wang XT (2018) Measurements of internal flow regime and bubble size in effervescent atomizer. *Exp Thermal Fluid Sci* 98:604–620
19. Sun CH, Ning Z, Lv M, Yan K, Fu J (2016) Acoustic performance of effervescent sprays by time-frequency method with different atomizer structures under different operating conditions. *Int J Multiph Flow* 82:35–48
20. Huang X, Wang X, Li G (2008) Visualization of two-phase flow inside an effervescent atomizer. *J Vis* 11(4):299–308
21. Zaremba M, Maly M, Jedelsky J et al (2018) An experimental analysis of the spraying processes in improved design of effervescent atomizer. *Int J Multiph Flow* 103:1–15
22. Ramamurthi K, Sarkar UK, Raghunandan BN (2009) Performance characteristics of effervescent atomizer in different flow regimes. *Atomiz Sprays* 19(1):41–56
23. Mohammadi A, Ommi F, Saboohi Z (2022) Experimental and numerical study of a twin-fluid two-phase internal-mixing atomizer. *J Therm Anal Calorim* 147(5):3673–3687
24. Li F, Lee C, Wang ZM, Liu FS, Lu GX (2020) Optical investigation on impacts of ambient pressure on macroscopic spray characteristics of ducted fuel injection under non-vaporizing conditions. *Fuel* 268:117192
25. Wang ZM, Dai XY, Liu FS, Li YF, Wu H, Wang CM, Li YK (2019) Microscopic study on the mechanisms for formation of the initial spray morphology. *Fuel* 235:715–722
26. Yu SH, Yin BF, Deng WX, Jia HK, Ye Z, Xu B, Xu HP (2018) Internal flow and spray characteristics for elliptical orifice with large aspect ratio under typical diesel engine operation conditions. *Fuel* 228:62–73
27. Mlkvik M, Jedelsky J, Karbstein HP, Gaukel V (2020) Spraying of viscous liquids: influence of fluid-mixing mechanism on the performance of internal-mixing twin-fluid atomizers. *Appl Sci* 10(15):5249
28. Wittner MO, Karbstein HP, Gaukel V (2019) Air-core-liquid-ring (ACLR) atomization: influences of gas pressure and atomizer scale up on atomization efficiency. *Processes* 7(3):139
29. Nielsen AF, Bertelsen P, Kristensen HG, Kristensen J, Hovgaard L (2006) Investigation and comparison of performance of effervescent and standard pneumatic atomizer intended for soluble aqueous coating. *Pharm Dev Technol* 11(2):243–253
30. Sovani SD, Sojka PE, Lefebvre AH (2001) Effervescent atomization. *Prog Energy Combust Sci* 27(4):483–521
31. Cejpeka O, Malya M, Dhinasekaran VK, Avulapati MM, Dacanay L, Jedelsky J (2023) Novel atomizer concept for CCS applications: impinging effervescent atomizer. *Sep Purif Technol* 311:123259
32. Xie J, Liu LS, Liu XC, Qu HR, Duan RZ (2022) Effect of bubble cutting on spray characteristics and dust control performance in the effervescent atomization. *Process Saf Environ Prot* 167:493–499
33. He XJ, Chen C, Yang Y, Yan ZH (2020) Experimental study on the flow field distribution characteristics of an open-end swirl injector under ambient pressure. *Aerosp Sci Technol* 98:105691
34. Chen C, He XJ, Liu CZ, Yang Y, Tang ZG (2021) Experimental study on the flow field distribution characteristics of a gas-liquid swirl coaxial injector under ambient pressure. *Aerosp Sci Technol* 114:106757
35. Chen C, Yang Y, Yang SH, Gao HL (2017) The spray characteristics of an open-end swirl injector at ambient pressure. *Aerosp Sci Technol* 67:78–87
36. Stähle P, Gaukel V, Schuchmann HP (2015) Comparison of an effervescent nozzle and a proposed air-core-liquid-ring (ACLR) nozzle for atomization of viscous food liquids at low air consumption. *J Food Process Eng* 40:1
37. He XJ, Yan ZH, Chen C, Qi XH (2019) Design and experiment of new air/ethanol torch igniter. *J Propul Technol* 40(11):2513–2520
38. Zaremba M, Weiß L, Mal M, Wensing M, Jedelsky J (2017) Low-pressure twin-fluid atomization: Effect of mixing process on spray formation. *Int J Multiphase Flow*. 89:277–289
39. Liu M, Duan YF, Zhang TN (2010) Evaluation of effervescent atomizer internal design on the spray unsteadiness using a phase/Doppler particle analyzer. *Exp Thermal Fluid Sci* 34(6):657–665
40. Liu M, Duan YF, Zhang TN, Xu YQ (2011) Evaluation of unsteadiness in effervescent sprays by analysis of droplet arrival statistics the influence of fluids properties and atomizer internal design. *Exp Thermal Fluid Sci* 35(1):190–198
41. Ma X, Duan Y, Liu M (2013) Atomization of petroleum-coke sludge slurry using effervescent atomizer. *Exp Thermal Fluid Sci* 46:131–138
42. Antonov DV, Shlegel NE, Strizhak PA (2020) Energy analysis of secondary droplet atomization schemes. *Int Commun Heat Mass Transfer* 117:3–9

Publisher's Note Springer Nature remains neutral with regard to jurisdictional claims in published maps and institutional affiliations.

Springer Nature or its licensor (e.g. a society or other partner) holds exclusive rights to this article under a publishing agreement with the author(s) or other rightsholder(s); author self-archiving of the accepted manuscript version of this article is solely governed by the terms of such publishing agreement and applicable law.